Hyperchaotic dynamics and synchronization of external-cavity semiconductor lasers

Volker Ahlers,* Ulrich Parlitz, and Werner Lauterborn
Drittes Physikalisches Institut, Universität Göttingen, Bürgerstraße 42-44, D-37073 Göttingen, Germany
(Received 15 May 1998)

Two unidirectionally coupled external cavity semiconductor lasers showing chaotic intensity fluctuations are studied by numerically solving the Lang-Kobayashi model equations [IEEE J. Quantum Electron. **QE-16**, 347 (1980)]. The systems are shown to synchronize when operating in the regime of low-frequency fluctuations, which is characterized by a very high-dimensional ($d>150$) attractor. The influence of parameter differences between the two lasers on the synchronization quality is investigated. [S1063-651X(98)02512-4]

PACS number(s): 05.45.+b, 42.55.Px, 42.65.Sf

I. INTRODUCTION

Synchronization phenomena are of fundamental importance for many physical, biological, and technical systems. Since the pioneering work by Fujisaka and Yamada [1], Pikovsky [2], and Afraimovich, Verichev, and Rabinovich [3], it has been known that even chaotic systems may synchronize. This aspect of nonlinear dynamics became an issue of great interest when Pecora and Carroll demonstrated synchronization of unidirectionally coupled chaotic systems [4] and suggested potential applications in communication systems. Examples of encoding methods based on chaos synchronization were presented in Ref. [5] using electronic circuits. Since many modern communication devices are optoelectronic or all optical, in this paper we address the question of chaos synchronization of unidirectionally coupled laser systems. Synchronization of chaotic lasers has been shown experimentally and numerically for Nd:YAG and CO_2 lasers (where YAG denotes yttrium aluminum garnet) [6]. Recently, synchronization of chaotic erbium-doped fiber ring lasers has been shown experimentally and numerically [7]. Of special interest in optical communication, however, is the semiconductor laser (SL), mainly due to its size and its possibility to be easily modulated [8]. A communication scheme based on synchronization of chaotic laser diodes with electro-optical feedback has recently been implemented experimentally [9].

External cavity semiconductor lasers (ECSLs) have been a subject of extensive research [10] during the past 15 years because of the importance of optical feedback phenomena in technical applications such as optical data storage or optical fiber communications. In most of these cases, one tries to avoid the effects of optical feedback. A typical effect due to feedback are low-frequency fluctuations (LFF's), which can be observed for moderate feedback and low pump current. This phenomenon has attracted considerable interest during the past few years. In particular, the question whether the underlying dynamics is (mainly) a stochastic process or governed by a chaotic attractor has been discussed very controversially [11–14]. The numerical simulations presented in Sec. II, which are based on deterministic model equations, show that the LFF dynamics correspond to a very high-dimensional chaotic attractor. This observation, together with recent experimental results [15] corroborating the deterministic model, indicates that LFFs are essentially a hyperchaotic deterministic process. Because of the high-dimensional attractor, the LFF signal is very difficult to distinguish from a stochastic signal.

In the following sections synchronization of ECSLs in the LFF regime is investigated by numerically solving the usual rate equations. Synchronization of ECSLs has previously been studied numerically using different coupling schemes [16,17]. The synchronization scheme employed in our simulations is similar to but different from that used in Ref. [16]. In particular, we consider a coupling that in principle allows perfect synchronization and also works if the driven laser does not possess an external cavity, which makes it easier to implement the scheme experimentally. Furthermore, the effects of parameter mismatch between both coupled lasers are studied in terms of unstable cw solutions embedded in the chaotic drive attractor.

II. HYPERCHAOTIC LASER DYNAMICS

The schematic setup of an ECSL is shown in Fig. 1. Light from the SL is reflected by the mirror and reinjected into the laser cavity.

To model the first ECSL, we use the well-known Lang-Kobayashi equations [18] for the complex electric field amplitude $E(t)$ (just behind the right laser facet) and the carrier number $N(t)$. These equations are generally considered to give a valid approximation of a single-mode SL with weak to moderate optical feedback from an external resonator. Writing $E(t)=E_0(t)\exp\{i[\omega_0 t+\phi(t)]\}$, splitting the complex equation for $E(t)$ into two real ones for the real amplitude $E_0(t)$ and the slowly varying phase $\phi(t)$, and using the carrier number above the value for the solitary SL (without an external resonator), $n(t)=N(t)-N_{\mathrm{sol}}$, these equations read [19,13]

FIG. 1. Schematic setup of an external cavity semiconductor laser (SL, semiconductor laser; *M*, mirror).

*Electronic address: vahlers@physik3.gwdg.de

TABLE I. Parameters used in the simulations. Values are taken from Ref. [13].

solitary laser carrier number	N_{sol}	1.707×10^{8}
differential optical gain	G_N	2.142×10^{4} s^{-1}
external cavity round-trip time	τ	10 ns
linewidth enhancement factor	α	5.0
carrier decay rate	γ	0.909 ns^{-1}
cavity decay rate	Γ	0.357 ps^{-1}
pump current relative to J_{th}	p	1.02
wavelength	$2\pi c/\omega_0$	635 nm
spontaneous emission rate	C_{sp}	10^{-5} s^{-1}

$$\frac{d}{dt}E_0(t)=\frac{1}{2}G_N n(t)E_0(t)+\frac{C_{\mathrm{sp}}\gamma[N_{\mathrm{sol}}+n(t)]^{-1}}{2E_0(t)}+\kappa E_0(t-\tau)\cos[\omega_0\tau+\phi(t)-\phi(t-\tau)], \quad (1)$$

$$\frac{d}{dt}\phi(t)=\frac{1}{2}\alpha G_N n(t)-\kappa\frac{E_0(t-\tau)}{E_0(t)}\times\sin[\omega_0\tau+\phi(t)-\phi(t-\tau)], \quad (2)$$

$$\frac{d}{dt}n(t)=(p-1)J_{\mathrm{th}}-\gamma n(t)-[\Gamma+G_N n(t)]E_0^2(t), \quad (3)$$

where we have included the average spontaneous emission rate C_{sp}. The exact value of the angular frequency ω_0 of the solitary laser is found to be of no importance for the qualitative results. We have chosen a value corresponding to a red laser diode. κ is the feedback rate and pJ_{th} is the pump current in units of the electron charge, where $J_{\mathrm{th}}=\gamma N_{\mathrm{sol}}$ is the threshold value of the solitary laser. The other parameters are explained in Table I; the values are taken from Ref. [13].

Equations (1)–(3) include delay differential equations. We used a fourth-order Runge-Kutta-Fehlberg integrator and a sixth-order Hermite interpolation scheme [20] for all numerical calculations presented in this paper. Results are shown in Fig. 2(a) for $\kappa=10^{10}$ s^{-1} and in Figs. 2(b) and 2(c) for $\kappa=10^{11}$ s^{-1}. In the latter case, the intensity breakdowns known as LFFs as well as the picosecond pulses [13,15] are observed.

In order to estimate the dimension of the underlying attractor a method introduced by Farmer [21] is used to calculate the largest Lyapunov exponents of the infinite-dimensional system. The ten largest Lyapunov exponents as a function of the feedback rate κ are shown in Fig. 3(a) for 10^{8} s$^{-1}\leqslant\kappa\leqslant10^{9}$ s^{-1} and in Fig. 3(b) for 10^{9} s$^{-1}\leqslant\kappa\leqslant10^{11}$ s^{-1}. As can be seen, the system is hyperchaotic for both values $\kappa=10^{10}$ and 10^{11} s^{-1}, which were used to calculate the time series shown in Fig. 2.

In order to characterize the dynamics of the LFFs in more detail the spectrum of the 150 largest Lyapunov exponents is shown in Fig. 4 for $\kappa=10^{11}$ s^{-1}. As can be seen, the first 150 exponents are positive or vanish. The Lyapunov dimension of the LFF attractor is thus larger than 150.

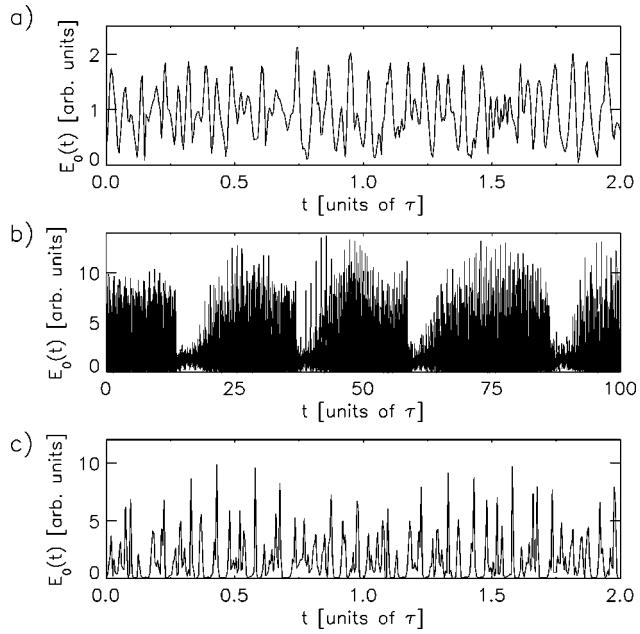

FIG. 2. Dynamics of the ECSL for (a) $\kappa=10^{10}$ s^{-1} and (b) and (c) $\kappa=10^{11}$ s^{-1}. Note the different scales of the axes.

III. UNIDIRECTIONALLY COUPLED SEMICONDUCTOR LASERS

The synchronization arrangement assumed for the simulations presented in this paper is shown in Fig. 5. It consists of two external cavity semiconductor lasers that are coupled unidirectionally via an optical diode, which can be realized experimentally using a Faraday isolator. In a real experimental situation, variable attenuators would be necessary to control feedback and coupling strengths. Coherent light from the first external cavity SL, the drive system, is injected into the

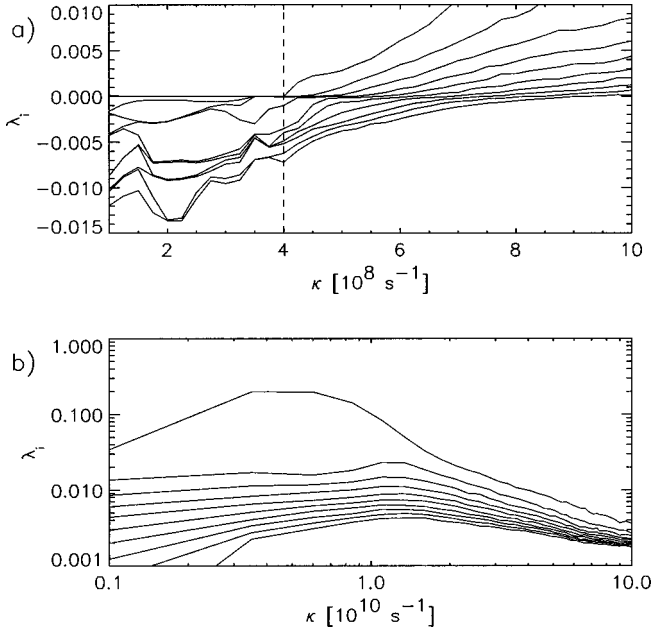

FIG. 3. Ten largest Lyapunov exponents λ_i of the ECSL for different values of the feedback rate κ. For $\kappa>4\times10^{8}$ s^{-1} the system is chaotic with an increasing number of positive Lyapunov exponents. Note the log-log scale in (b).

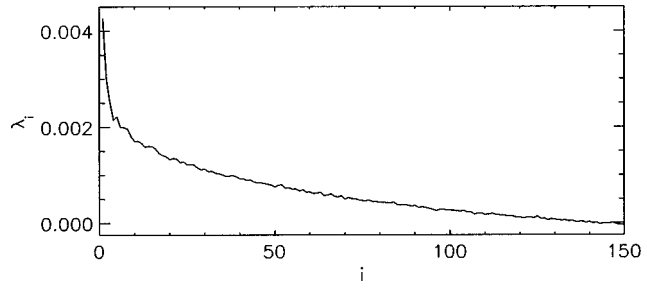

FIG. 4. Spectrum of the 150 largest Lyapunov exponents λ_i for the LFF attractor ($\kappa = 10^{11}\ \mathrm{s}^{-1}$).

second external cavity SL, the response system.

The light that is injected into the second system through coupling is included in the equations in a way similar to the light coming from the external resonator. This approach is widely used to describe the effects of coherent light injection into semiconductor lasers [22]. The equations for the second system thus read

$$\frac{d}{dt}\tilde{E}_0(t) = \frac{1}{2}G_N\tilde{n}(t)\tilde{E}_0(t) + \frac{C_{\mathrm{sp}}\gamma[N_{\mathrm{sol}}+\tilde{n}(t)]}{2\tilde{E}_0(t)} + \tilde{\kappa}\tilde{E}_0(t-\tau) \times\cos[\omega_0\tau+\tilde{\phi}(t)-\tilde{\phi}(t-\tau)] + \sigma E_0(t-\tau_c)\cos[\omega_0\tau_c+\tilde{\phi}(t)-\phi(t-\tau_c)], \quad (4)$$

$$\frac{d}{dt}\tilde{\phi}(t) = \frac{1}{2}\alpha G_N\tilde{n}(t) - \tilde{\kappa}\frac{\tilde{E}_0(t-\tau)}{\tilde{E}_0(t)}\sin[\omega_0\tau+\tilde{\phi}(t)-\tilde{\phi}(t-\tau)] - \sigma\frac{E_0(t-\tau_c)}{\tilde{E}_0(t)}\sin[\omega_0\tau_c+\tilde{\phi}(t)-\phi(t-\tau_c)], \quad (5)$$

$$\frac{d}{dt}\tilde{n}(t) = (p-1)J_{\mathrm{th}} - \gamma\tilde{n}(t) - [\Gamma + G_N\tilde{n}(t)]\tilde{E}_0^2(t), \quad (6)$$

where σ is the coupling strength and τ_c is the time the light needs to travel from the right facet of the first SL to the right facet of the second one. Note the difference between $E_0(t), \phi(t)$ and $\tilde{E}_0(t), \tilde{\phi}(t)$, describing the electric fields in the drive and the response lasers, respectively.

Synchronization is possible if there exists a solution of Eqs. (1)–(3) and (4)–(6) with

$$\tilde{E}_0(t) = E_0(t-\Delta t),$$

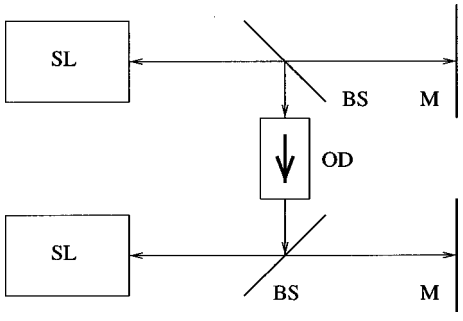

FIG. 5. Synchronization arrangement (SL, semiconductor laser; *M*, mirror; BS, beam splitter; OD, optical diode).

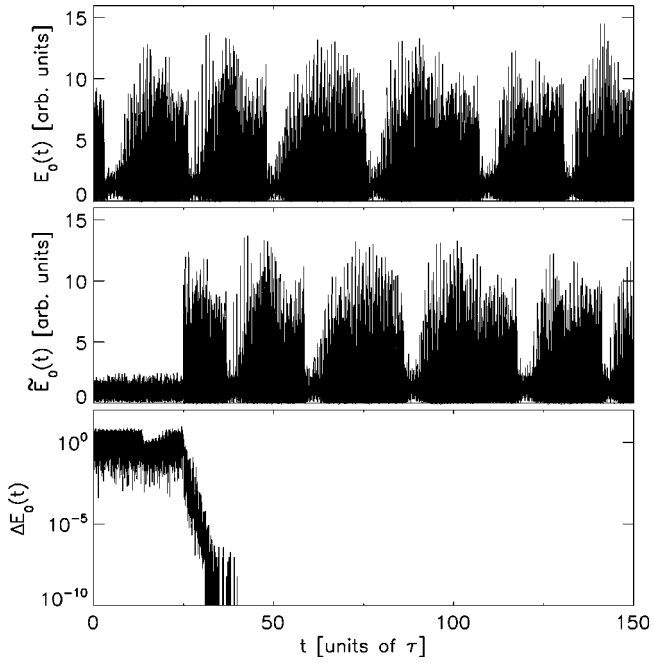

FIG. 6. Synchronization of drive and response lasers in the LFF regime. Plotted are the electric field amplitudes $E_0(t)$ and $\tilde{E}_0(t)$ of drive and response, respectively, and their normalized difference $\Delta E_0(t) = |\tilde{E}_0(t) - E_0(t-\Delta t)|/\langle E_0(t)\rangle$. Due to time delays the intensity signal $\tilde{E}_0(t)$ of the response laser is shifted in time with respect to the drive by $\Delta t = \tau_c - \tau = 1.058\,33\times10^{-7}$ s $= 10.5833\tau$. The parameters of the lasers are given in Table I and are assumed to be exactly the same for both systems with a coupling given by $\kappa = 10^{11}\ \mathrm{s}^{-1}$, $\tilde{\kappa} = 10^{10}\ \mathrm{s}^{-1}$, and $\sigma = 9\times10^{10}\ \mathrm{s}^{-1}$.

$$\tilde{\phi}(t) = \phi(t-\Delta t) - \omega_0\Delta t \pmod{2\pi},$$

$$\tilde{n}(t) = n(t-\Delta t),$$

where $\Delta t = \tau_c - \tau$ accounts for the time delay of the synchronization introduced through τ_c. A synchronous solution exists if

$$\kappa = \tilde{\kappa} + \sigma. \quad (7)$$

This condition can be realized by adjusting the coupling and feedback strengths. Equation (7) includes the possibility of the response system consisting of a solitary SL, i.e., $\tilde{\kappa} = 0\ \mathrm{s}^{-1}$; in this case the feedback strength of the first system and the coupling strength have to be equal, $\kappa = \sigma$.

IV. SYNCHRONIZATION OF IDENTICAL LASERS

Equation (7) provides a necessary condition for synchronization; it does not tell, however, anything about the stability of the synchronized solution. Therefore, Eqs. (1)–(3) and (4)–(6), which include delay differential equations, have to be solved numerically.

Figure 6 shows the results for $\kappa = 10^{11}\ \mathrm{s}^{-1}$, $\tilde{\kappa} = 10^{10}\ \mathrm{s}^{-1}$, and $\sigma = 9\times10^{10}\ \mathrm{s}^{-1}$. For this feedback strength the drive laser is in the LFF regime [13], while the

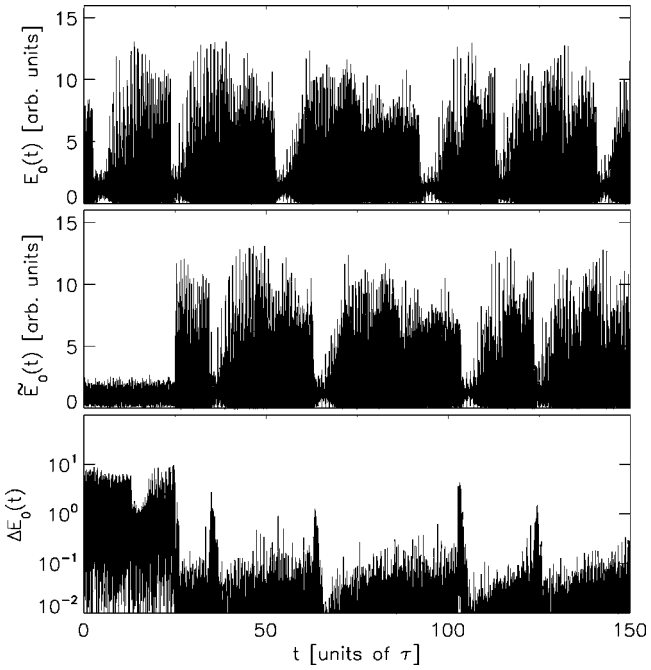

FIG. 7. Synchronization of drive and response systems with slightly different parameters for $\kappa=10^{11}$ s^{-1}, $\tilde{\kappa}=10^{10}$ s^{-1}, and $\sigma=9\times10^{10}$ s^{-1} (compare Fig. 6).

response laser is in another hyperchaotic state without coupling (compare Figs. 2 and 3). Plotted are the electric field amplitudes $E_0(t)$ and $\tilde{E}_0(t)$ for the drive and the response laser, respectively, as well as the synchronization error, which is defined as

$$\Delta E_0(t)=\frac{|\tilde{E}_0(t)-E_0(t-\Delta t)|}{\langle E_0(t)\rangle}, \tag{8}$$

where $\langle E_0(t)\rangle$ is the temporal average of the electric field amplitude of the drive laser.

At $t=25\tau$, the coupling is switched on. Synchronization occurs after some transient time. The electric field amplitude of the response laser then follows the amplitude of the drive laser with a time delay of $\Delta t=\tau_c-\tau$, which is taken into account in the definition (8) of the synchronization error. As can be seen from Fig. 6, nearly perfect synchronization is achieved. Similar results have been obtained for the case of a response laser without an external resonator ($\tilde{\kappa}=0$ s^{-1}), with the difference that shorter transient times are observed before perfect synchronization occurs.

V. SYNCHRONIZATION OF NONIDENTICAL LASERS

Since in practice no lasers are identical, those parameters of the response laser that cannot be adjusted (i.e., G_N, α, γ, Γ, and C_{sp}) have been varied randomly within 1.0% difference from the drive laser values. Figure 7 shows a typical result. As expected, no perfect synchronization is achieved, but over long times the systems synchronize in a less perfect way. During the intensity breakdowns, however, the systems desynchronize. Synchronization is regained when the electric field amplitude rises again. This can also be seen in Fig. 8, where the amplitude $\tilde{E}_0(t)$ of the response laser is plotted vs

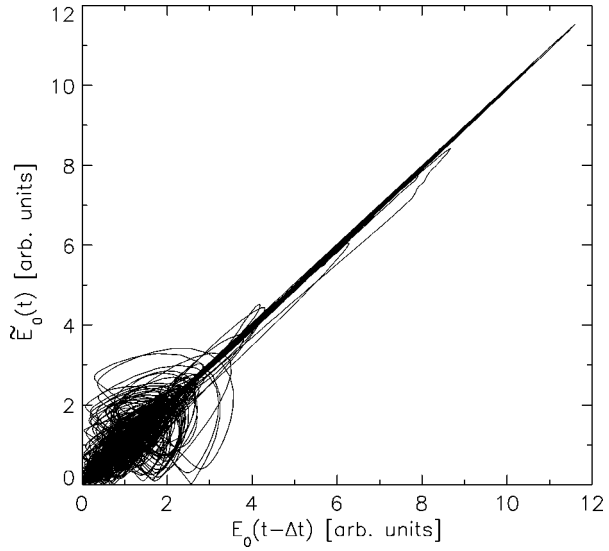

FIG. 8. Response amplitude $\tilde{E}_0(t)$ vs drive amplitude $E_0(t-\Delta t)$ shifted in time. For large E_0 synchronized dynamics along the diagonal occurs, but during intensity breakdowns of the drive both lasers desynchronize. The parameters are the same as in Fig. 7.

the amplitude $E_0(t-\Delta t)$ of the driving laser shifted in time. Perfect synchronization would lead to a motion along the diagonal, but here deviations (''excursions'') occur mainly for small values of the driving amplitude E_0.

The desynchronization during the intensity breakdowns does not affect their joint occurrence. Figure 9 shows the time traces of the intensity $P(t)=E_0^2(t)$ that would be observed in an experimental situation using a photodiode with finite detection time; the original amplitude traces from Fig. 7 have been squared and averaged over 5 ns. On a ''mac-

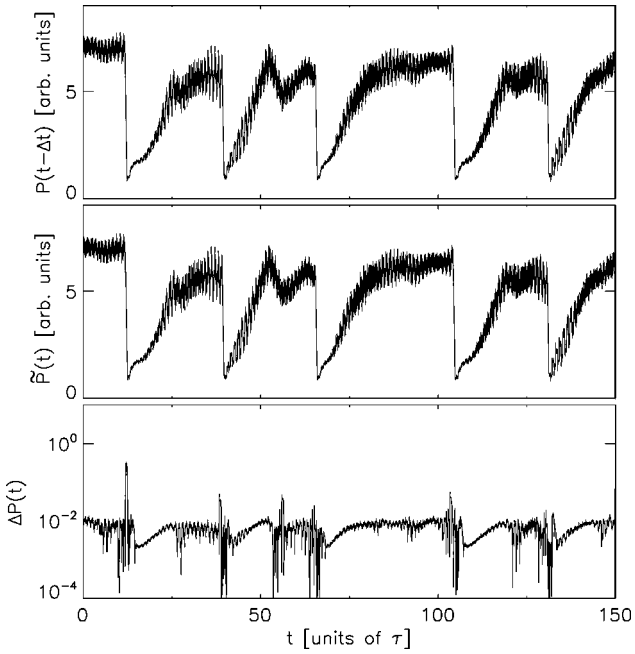

FIG. 9. Same parameters as in Fig. 7 but intensities $P(t)=E_0^2(t)$ averaged over 5 ns to take into account finite detection time. Note that $P(t-\Delta t)$ is plotted including the time shift Δt to demonstrate the simultaneous occurrences of the intensity breakdowns.

roscopic'' scale the systems synchronize quite well, including the occurrence of the intensity breakdowns. Their intensities differ, however, on a ''microscopic'' scale.

VI. UNSTABLE PERIODIC ORBITS

Short events of desynchronization such as those shown in Fig. 7 are typical for weakly coupled systems in the presence of noise or parameter mismatch [23]. The origin of this so-called *bubbling* phenomenon are unstable invariant subsets [such as unstable fixed points (UFPs) or unstable periodic orbits (UPOs)] of the drive attractor that fail to entrain the corresponding fixed point or periodic orbit of the response system. When driven with one of these UFPs or UPOs the response system does not synchronize, but oscillates in a different way from the drive. In the joint state space of drive and response these UFPs and UPOs are transversally unstable, i.e., in their vicinity the manifold containing the synchronized dynamics is repelling and not attracting. Whenever an almost synchronized trajectory comes close to a transversally unstable UFP or UPO it is repelled from the synchronization manifold and synchronization breaks down for a short period of time until the trajectory (re)enters a region where the synchronization manifold is attracting again. This mechanism explains also the intermittent character of the desynchronization bursts shown in Fig. 7. In order to investigate this source of synchronization breakdown for the coupled laser system we have studied the transversal (in)stability of unstable fixed points (i.e., cw solutions). A stationary (cw) solution of Eqs. (1)–(3) has a complex electric field

$$E(t)=E_0^s\exp(i\omega^s t+\phi_0)$$

and a carrier number

$$n(t)=n^s,$$

where $\omega^s=\omega_0+\Delta\omega$ is the angular light frequency that is shifted from the value ω_0 of the solitary laser by an amount $\Delta\omega$. For the slowly varying phase $\phi(t)$ it follows that $\phi(t)=\Delta\omega t+\phi_0$, so that the phase difference $\eta(t)=\phi(t)-\phi(t-\tau)$ is constant,

$$\eta^s=\Delta\omega\tau.$$

Substituting E_0^s, n^s, and η^s in Eq. (1) and neglecting spontaneous emission, we obtain

$$n^s=-\frac{2\kappa}{G_N}\cos(\omega_0\tau+\eta^s).$$

Using this in Eq. (2), we obtain an equation for η^s,

$$\eta^s+\kappa\tau\sqrt{1+\alpha^2}\sin(\omega_0\tau+\eta^s+\arctan\alpha)=0, \qquad (9)$$

which can only be solved numerically [8]. Solutions of Eq. (9) with positive derivative

$$1+\kappa\tau\sqrt{1+\alpha^2}\cos(\omega_0\tau+\eta^s+\arctan\alpha)>0$$

have been shown to be unstable foci and are generally referred to as *external cavity modes*, while solutions with negative derivative are saddle points and are called *antimodes* [10]. From Eq. (3) we finally obtain

$$E_0^s=\sqrt{\frac{(p-1)J_{\rm th}-\gamma n^s}{\Gamma+G_N n^s}}. \qquad (10)$$

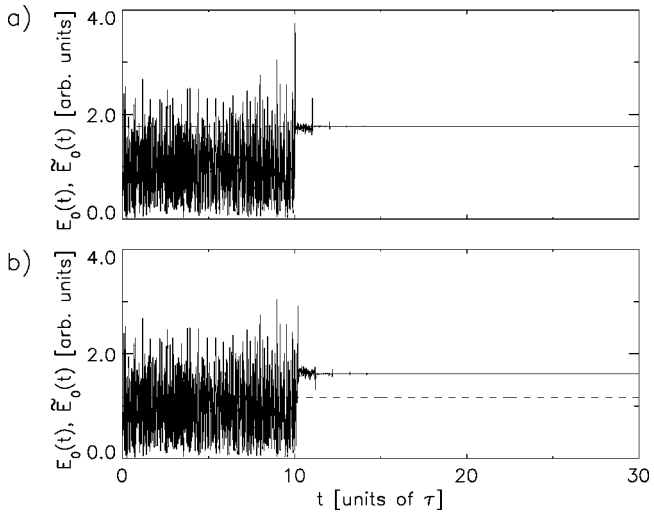

FIG. 10. Electric field amplitudes of drive (dashed line) and response (solid line) lasers when the response system is driven with (a) an external cavity mode and (b) an antimode, respectively. At $t=10\tau$ the coupling is switched on. The parameters are the same as in Fig. 6.

The process of LFFs has been explained in the following way [12,13]. During the intensity buildup phase, the system oscillates in the vicinity of the (unstable) foci. From time to time, it moves from one focus to the next, preferably in the direction of decreasing values of η^s. At some point, the system comes too close to a saddle point and is carried away by its unstable manifold. This leads to an intensity breakdown, after which the buildup phase recommences.

To investigate the hypothesis that unstable periodic orbits might be the reason for the loss of synchronization during the intensity breakdowns, we used stationary solutions [which are fixed points of the system (E_0,η,n)] of the drive system to drive an identical response system. For this task, the value of η^s was calculated by numerically solving Eq. (9) and then the value for E_0^s from Eq. (10) and the phase $\phi(t)=\eta^s t/\tau$ were used as drive variables in Eqs. (4)–(6). The parameters were the same as in Sec. IV. The systems synchronize when an unstable focus is used to drive the response system, as can be seen in Fig. 10(a). When a saddle point is used as a drive, however, no synchronization is achieved [cf. Fig. 10(b)]. In this case the response system also generates cw output, but at a different value of the electric field amplitude $\tilde{E}_0(t)$.

When the system comes too close to a saddle point, two independent events take place. First, the average intensity of the drive system breaks down and the value of the inversion $n(t)$ increases very rapidly due to the saddle node instability. Second, the synchronization between the drive and the response systems is lost because of the desynchronizing property of the saddle point. When the drive system has left the vicinity of the saddle point, synchronization is regained.

Since the unstable foci do not have that desynchronizing property, they are of no danger for the synchronization. This mechanism also explains the occurrence of desynchronization events at *low* drive intensities P (see Figs. 7 and 8) because all unstable cw solutions have amplitudes $E_0^s < 3$ (arbitrary units), as can be computed using Eq. (10).

VII. CONCLUSION

In this paper we have presented numerical simulations of synchronizing hyperchaotic semiconductor lasers that are unidirectionally coupled by their electric fields. For perfectly identical lasers the synchronization error converges to zero very rapidly, but (slight) parameter mismatch leads to intermittent breakdown of the synchronization, i.e., the difference of the electric field amplitudes of drive and response lasers becomes rather large for short periods of time. The main reason for these desynchronization events is the existence of transversally unstable cw solutions that are embedded in the chaotic attractor. Although these results indicate that one may not obtain ''high-quality'' synchronization in experimental implementations (where noise and parameter mismatch are unavoidable), such a setup nevertheless may be useful for practical applications because the synchronization breakdowns coincide with intensity breakdowns. Therefore, the envelope of the intensity fluctations of the driving laser is well reproduced by the response laser even in the case of parameter mismatch and despite the very high dimension ($d > 150$) of the underlying chaotic attractor. If this envelope is of importance (for example, in a chaos-based communication system) then the ''low-quality'' synchronization observed with parameter mismatch may be sufficient.

ACKNOWLEDGMENTS

We thank L. Kocarev, L. Junge, R. Roy, H. D. I. Abarbanel, N. Rulkov, M. Sushchick, and our colleagues and the technical staff of the Third Physical Institute for stimulating discussions on chaos synchronization and support. This work was supported by the Deutsche Forschungsgemeinschaft (Project No. Pa 643/1-1).

[1] H. Fujisaka and T. Yamada, Prog. Theor. Phys. **69**, 32 (1983); **70**, 1240 (1983).
[2] A. S. Pikovsky, Z. Phys. B **55**, 149 (1984).
[3] V. S. Afraimovich, N. N. Verichev, and M. I. Rabinovich, Radiophys. Quantum Electron. **29**, 795 (1986).
[4] L. M. Pecora and T. L. Carroll, Phys. Rev. Lett. **64**, 821 (1990).
[5] K. M. Cuomo and A. V. Oppenheim, Phys. Rev. Lett. **71**, 65 (1993); L. Kocarev and U. Parlitz, *ibid.* **74**, 5028 (1995); U. Parlitz, L. Kocarev, T. Stojanovski, and H. Preckel, Phys. Rev. E **53**, 4351 (1996); M. de Sousa Vieira, P. Khoury, A. J. Lichtenberg, M. A. Lieberman, W. Wonchoba, J. Gullicksen, J. Y. Huang, R. Sherman, and M. Steinberg, Int. J. Bifurcation Chaos Appl. Sci. Eng. **2**, 645 (1992); N. F. Rulkov, A. R. Volkovskii, A. Rodriguez-Lozano, E. Del Rio, and M. G. Velgarde, *ibid.* **2**, 669 (1992); L. Kocarev, K. S. Halle, K. Eckert, L. O. Chua, and U. Parlitz, *ibid.* **2**, 709 (1992).
[6] R. Roy and K. S. Thornburg, Phys. Rev. Lett. **72**, 2009 (1994); T. Sugawara, M. Tachikawa, T. Tsukamoto, and T. Shimizu, *ibid.* **72**, 3502 (1994); P. Colet and R. Roy, Opt. Lett. **19**, 2056 (1994).
[7] G. D. VanWiggeren and R. Roy, Science **279**, 1198 (1998); H. D. I. Abarbanel and M. B. Kennel, Phys. Rev. Lett. **80**, 3153 (1998).
[8] G. P. Agrawal and N. K. Dutta, *Semiconductor Lasers*, 2nd ed. (Van Nostrand Reinhold, New York, 1993),
[9] J.-P. Goedgebuer, L. Larger, and H. Porte, Phys. Rev. Lett. **80**, 2249 (1998).
[10] G. H. M. van Tartwijk and D. Lenstra, Quantum Semiclassic. Opt. **7**, 87 (1995).
[11] J. Sacher, W. Elsäßer, and E. O. Göbel, Phys. Rev. Lett. **63**, 2224 (1989).
[12] T. Sano, Phys. Rev. A **50**, 2719 (1994).
[13] G. H. M. van Tartwijk, A. M. Levine, and D. Lenstra, IEEE J. Sel. Top. Quantum Electron. **1**, 466 (1995).
[14] C. H. Henry and R. F. Kazarinov, IEEE J. Quantum Electron. **QE-22**, 294 (1986); A. Hohl, H. J. C. van der Linden, and R. Roy, Opt. Lett. **20**, 2396 (1995); M. Giudici, C. Green, G. Giacomelli, U. Nespolo, and J. R. Tredicce, Phys. Rev. E **55**, 6414 (1997); D. W. Sukow, J. R. Gardner, and D. J. Gauthier, Phys. Rev. A **56**, R3370 (1997).
[15] I. Fischer, G. H. M. van Tartwijk, A. M. Levine, W. Elsäßer, E. Göbel, and D. Lenstra, Phys. Rev. Lett. **76**, 220 (1996); I. Fischer, T. Heil, M. Münkel, and W. Elsäßer, Proc. SPIE **3283**, 63 (1998).
[16] C. R. Mirasso, P. Colet, and P. García-Fernández, IEEE Photonics Technol. Lett. **8**, 299 (1996).
[17] V. Annovazzi-Lodi, S. Donati, and A. Sciré, IEEE J. Quantum Electron. **33**, 1449 (1997).
[18] R. Lang and K. Kobayashi, IEEE J. Quantum Electron. **QE-16**, 347 (1980).
[19] J. Mørk, B. Tromborg, and J. Mark, IEEE J. Quantum Electron. **28**, 93 (1992).
[20] H. J. Oberle and H. J. Pesch, Numer. Math. **37**, 235 (1981); W. H. Press, S. A. Teukolsky, W. T. Vetterling, and B. P. Flannery, *Numerical Recipes in C: The Art of Scientific Computing*, 2nd ed. (Cambridge University Press, Cambridge, 1992), Sec. 16.2; J. Stoer and R. Bulirsch, *Introduction to Numerical Analysis* (Springer-Verlag, New York, 1980), Sec. 2.1
[21] J. D. Farmer, Physica D **4**, 366 (1982).
[22] R. Lang, IEEE J. Quantum Electron. **QE-18**, 976 (1982).
[23] D. J. Gauthier and J. C. Bienfang, Phys. Rev. Lett. **77**, 1751 (1996); N. Gupte and R. E. Amritkar, Phys. Rev. E **48**, R1620 (1993); L. Pecora, T. Carroll, and J. Heagy, Proc. SPIE **2612**, 25 (1995); P. Ashwin, J. Buescu, and I. Stewart, Phys. Lett. A **193**, 127 (1994); S. Venkataramani, B. Hunt, and E. Ott, Phys. Rev. E **54**, 1346 (1996); Y.-C. Lai, C. Grebogi, J. A. Yorke, and S. Venkataramani, Phys. Rev. Lett. **77**, 55 (1996); J. F. Heagy, T. L. Carroll, and L. M. Pecora, Phys. Rev. E **52**, R1253 (1996).